Network structure in alteration layer of boroaluminosilicate glass formed by aqueous corrosion

Huseyin Kaya[1], Dien Ngo[2], Nicholas J. Smith[3], Stephane Gin[4], and Seong H. Kim[1,2]*

1. Department of Materials Science and Engineering, The Pennsylvania State University, University Park, 16802, USA
2. Department of Chemical Engineering and Materials Research Institute, The Pennsylvania State University, University Park, PA 16802, USA
3. Science and Technology Division, Corning Incorporated, Corning, NY 14830, USA
4. CEA, DES, ISEC, DE2D, University of Montpellier, Marcoule, F-30207 Bagnols sur Cèze, France

*Corresponding author: shkim@engr.psu.edu, shk10@psu.edu

Abstract

Exogenously-added LiCl has been shown to slightly accelerate the corrosion rate of a boroaluminosilicate glass in aqueous solutions over forward- and residual-rate regimes, while KCl and CsCl impede. To understand the effect of exogenously added electrolytes on resulting hydrous species and the network structure of alteration layers, infrared spectroscopy was implemented. It was found that the fraction of molecular water over the surface-bound hydroxyl species is lower in the KCl and CsCl conditions compared to the LiCl and pure water conditions. An approximation for the spectral features of the thin surface films from an experimentally-obtained spectrum in specular-reflectance infrared (SR-IR) spectroscopy was proposed; results indicate no significant difference in the Si-O bonding network of the alteration layers formed in the presence of exogenously added LiCl, KCl and CsCl. The observed change in rates might be linked to the relative abundance of molecular water species in the porous network, rather than the silicate bonding structure.

1. Introduction

To predict long term stability of vitrified nuclear wastes in underground repository facilities, factors affecting glass corrosion in aqueous conditions need to be fully explored. Aqueous corrosion of glass does not proceed by a single mechanism with a fixed rate, but it occurs through a set of multiple processes with varying rates that evolve differently over time and manifest in a complex way depending on corrosion conditions. Under static conditions, glass corrosion rates tend to decrease and eventually reach a steady state with a very slow residual rate as the surrounding solution approaches saturation of certain elements, and this is often accompanied by the formation of transport-limiting corroded surface layers.[1-5] These surface layers, also called alteration layers, are found to be porous[6, 7] and such pores are due to dissolution of modifier ions (Na and part of Ca) and glass network formers (mostly B) followed by network re-organization through condensation of hydroxylated network.[8-10] The corrosion rate observed depends on a host of factors, including the composition, thermal history, and surface preparation of glass samples, as well as temperature and pH of the corrosion solution, the sample surface area to solution volume (S/V) ratio, near-field materials, and so on.[4, 11-16] The presence of exogenous electrolyte ions in the corrosion solution have also been shown to affect the glass corrosion kinetics in both (initial) forward rate and (steady state) residual rate regimes,[9, 17-20] but how they affect the glass corrosion behavior is not well understood. In the residual rate regime, one possible hypothesis is that the electrolyte ions in solution can diffuse into the corroded surface layer and eventually lead to the alteration of the network structure within the layer. This might occur if the intruding ions alter the chemical potential of reactive species, such as the affinity of local binding sites for water on the internal pore surfaces; disruption of the hydrogen bonding network of water molecules within pores; and/or changes to the stability of other ions dissolved in the structured water inside the pores, etc. Thus, the ability to analyze the network structure of corroded glass surface layers is critically needed for better understanding of glass corrosion mechanisms in aqueous environments, and in particular to help to address this hypothesis related to the impact of exogeneous electrolyte ions.

The structural information of the glass network can be obtained, in theory, using X-ray or neutron scattering, nuclear magnetic resonance (NMR), and vibrational spectroscopy.[21-31] However, conventional scattering and NMR techniques are not highly surface sensitive;[32, 33]

thus, unless the sample size is on the same order of the corroded layer thickness, the bulk signal will dominate over the surface signal. One way of overcoming this limitation would be to use fine powders produced by crushing and sieving for corrosion experiments.[9] But, the corrosion behavior under non-equilibrium conditions can be different for mechanically-fractured or crushed surfaces with substantial subsurface damage versus thermally-produced surfaces (such as cooling from the melt or annealing) that contain fewer subsurface structural defects.[13, 34, 35]

Compared to the scattering and NMR techniques, vibrational spectroscopy is inherently more surface sensitive if the analysis is performed in the reflection mode, such as with specular reflection infrared (SR-IR) spectroscopy or attenuated total reflection infrared (ATR-IR) spectroscopy.[36, 37] These methods are readily applicable to monolithic and optically-flat glass surfaces. Even so, the ATR-IR method does not work well for the direct analysis of silicate network vibrations due to limitations associated with the complex refractive index ($n(\lambda) + ik(\lambda)$) of glass with an extremely high absorptivity ($\alpha(\lambda) = 4\pi k(\lambda)/\lambda$) in the wavelength (λ) region corresponding to the absorption of the Si-O network vibrations.[38] Although this high absorptivity is problematic for ATR-IR analysis, it is substantially responsible for the good surface sensitivity observed in SR-IR analysis. It should be noted that the SR-IR probe depth varies drastically in the network vibration region due to the wavelength dependence of absorptivity.[38, 39] If the corrosion layer is much thicker than the effective probe depth over the entire spectral region, the contribution from the pristine bulk would be negligible. On the contrary, if the altered layer is thinner than the probe depth, the measured SR-IR spectrum will be a convolution of both surface and bulk signals, with relative contributions that vary with IR wavelength. In most glass corrosion studies conducted in environmentally-relevant aqueous conditions for nuclear waste disposal, the corrosion layer thickness has been found as around a few microns, which is not necessarily thick enough to safely neglect bulk contributions.[8, 40, 41] Thus, without proper deconvolution of the bulk contribution, it is difficult to obtain accurate information on the network structure of the corroded layer directly from SR-IR analysis.

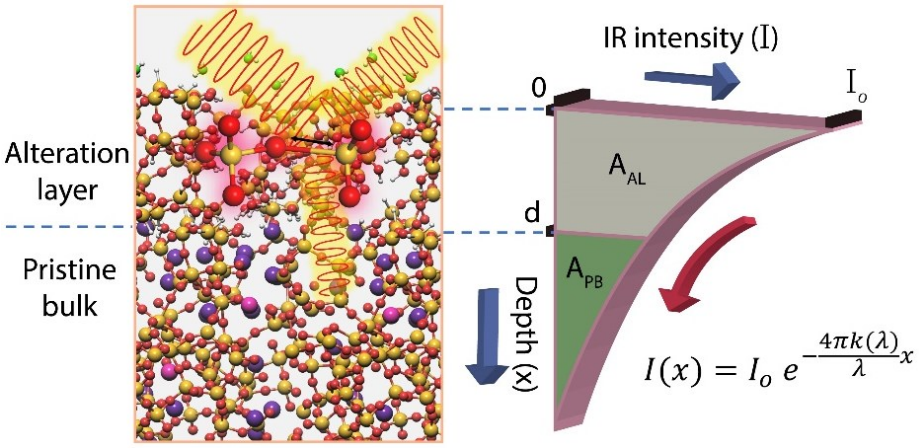

Figure 1. Illustration of interaction between an IR electric field and a corroded glass surface. The IR electric field attenuates exponentially from the outermost surface and the spectrum obtained can have contributions from both the altered layer and pristine bulk. I_o is electric field intensity at the outermost surface, d is the thickness of alteration layer, λ is wavelength, and k is the imaginary part of complex refractive index.

In this paper, we propose a simple mathematical algorithm as a facile approximation method to subtract the bulk contribution in the SR-IR analysis and estimate the vibrational spectral features of the glass network in the surface alteration layer (Figure 1). This method was then employed for structural analysis of the altered layers formed on International Simple Glass (ISG) after exposure to aqueous solutions containing different cations. ISG is a model boroaluminosilicate glass containing sodium and calcium modifier ions, as well as a minor amount of zirconium, and was proposed for round-robin studies of glass corrosion mechanisms relevant to environmental degradation of glasses used for immobilization of radio-active nucleotides.[3] The electrolyte condition of aqueous solutions was chosen in reference to a previous publication for direct comparison with the solution analysis data.[9] The algorithm for deconvolution of the bulk contribution is based on the fact that the IR intensity is exponentially attenuated by absorption inside the sample (Figure 1). The algorithm discussed in this paper requires knowledge of the refractive index of both the corrosion layer and the bulk glass over the IR wavelength span of interest, as well as the thickness of the corrosion layer. The refractive index of the corrosion layer could be obtained from infrared variable-angle spectroscopic ellipsometry (IR-VASE) analysis of a thick alteration layer.[42, 43] The thickness of the altered layer can be determined using spectroscopic ellipsometry (SE), secondary ion mass spectrometry (SIMS) depth profiling, scanning electron microscopy (SEM) cross-section imaging or estimated from mass balance using

the measured concentrations of glass components dissolved into a corrosion solution.[4, 7, 44] The refractive index of the bulk glass can be obtained with IR-VASE or using the two-angle SR-IR method.[45] Note that the algorithm discussed here is an approximation method with some limitations in its validity and accuracy. Even with these limitations, it was found that the application of this method and comparison with the IR-VASE data can provide the structural information of the Si-O bonding network in the alteration layer formed on ISG samples. In addition, the relative abundance of hydrous species in the alteration layer was analyzed with attenuated total reflectance infrared (ATR-IR) spectroscopy analysis probing hydrous species. The comparison of these analysis provides an insight into key parameters affecting the glass corrosion behavior.

2. Experimental details

2.1. Sample preparation

ISG samples (60.2 SiO_2, 16.0 B_2O_3, 12.6 Na_2O, 5.7 CaO, 3.8 Al_2O_3 and 1.7 ZrO_2 in mol%)[3, 46] were cut into coupons (1 cm × 1 cm × 0.2 cm) from an ISG block (produced by MoSci Corp.). One large face of each coupon was polished to an optical finish while the other large face was left as-cut and visibly rough to mitigate the detrimental effects of backside reflection in SE measurements.[47] The coupons were corroded under static conditions without any agitation at 90 °C in aqueous solutions initially saturated with soluble silica species prepared following the protocol provided in the literature.[40] The $pH^{90°C}$ of the corrosion solutions was held at 7±0.5 during the experiment. Eight coupons were immersed in 350 mL solutions in 500 mL perfluoroalkoxy jars and the initial geometrical surface area to solution volume ratio (S/V) was 6.4 m^{-1}. The corrosion solutions had ~5 mmol/L of soluble silicon-containing species and ~0.13 mmol/L of Li^+, K^+ and Cs^+ ions depending on the electrolyte condition.[7] The corrosion condition with no added electrolytes is referred to as NAE hereafter. Prior works have shown that B, Na, and Ca leach from ISG under these conditions, leaving a nano-porous silica-rich layer mostly made of O, Si, Al and Zr.[40, 41, 48] This modification happens isovolumetric; the volume of formed alteration layer is equal to the volume of initially occupied by the pristine ISG.[8]

2.2. Specular reflection infrared (SR-IR) spectroscopy

SR-IR measurements were conducted using a Bruker Hyperion 3000 FT-IR spectrometer equipped with a 15x reflective objective, which has incident and collection angles ranging from 11.3° to 23.6° and an aperture size of 100 μm × 100 μm. The spectrum of a gold surface was used as the reference. Spectra were obtained by averaging 400 scans with a resolution of 6 cm^{-1}. The effective penetration depth of IR can be defined as the depth at which the IR intensity is attenuated to e^{-1} (i.e. attenuated by 63% compared to the intensity at the surface):[49]

$$d_p(\lambda) = \frac{\lambda}{\alpha(\lambda)} cos\theta \quad (1)$$

where λ is the IR wavelength, $\alpha(\lambda) = \frac{4\pi}{\lambda} \cdot k(\lambda)$ with k being the imaginary part of the refractive index of corroded ISG at the wavelength λ, and θ is the incident angle from the surface normal axis. In the calculation, an average θ of 18° was used for the incident angle. The effective probe depth can be defined as three times the penetration depth (= $3 \times d_p(\lambda)$).

Depending on the thickness of the altered layer, the measured IR spectrum can have contributions from both the altered layer and the underlying pristine bulk ISG. In a strict sense, when both contributions are present, the measured SR-IR spectrum will be dictated by the interference of IR beams reflected from multiple interfaces of all layers with different optical constants (n, k) between the air and the pristine glass bulk. As a simple approximation, one could assume that the SR-IR spectrum is comprised of the weighted sum of the alteration layer and bulk contributions:

$$I_{measured}(\omega) = I_{AL}(\omega) + I_{bulk}(\omega) \quad (2)$$

where $I_{measured}$ is the SR-IR spectral intensity at a given wavenumber ($\omega = 1/\lambda$), and I_{AL} and I_{bulk} are the contributions from the altered layer and the pristine bulk, respectively. The I_{bulk} contribution could be estimated considering the exponential decay of IR intensity in the sample:

$$I_{bulk}(\omega) = I_{m,bulk}(\omega) \times \left(\frac{A_{bulk}(\omega)}{A_{AL}(\omega) + A_{bulk}(\omega)}\right) \quad (3)$$

where $I_{m,bulk}(\omega)$ is the SR-IR intensity of the *uncorroded* sample measured at the wavenumber ω, and $A_{AL}(\omega)$ and $A_{bulk}(\omega)$ are fractions of the IR beam attenuated in the alteration layer and the pristine glass, respectively, as it propagates from the surface to the bulk (Figure 1). $A_{AL}(\omega)$

and $A_{bulk}(\omega)$ can be calculated by integrating the IR intensities along the corresponding portions of the attenuation curve:

$$A_{AL}(\omega) = I_o \int_0^d e^{-\frac{\alpha_{AL}(\lambda)}{\lambda}x} dx \quad (4)$$

$$A_{bulk}(\omega) = \left(I_o \times e^{-\frac{\alpha_{AL}(\lambda)}{\lambda}d}\right) \int_d^\infty e^{-\frac{\alpha_{bulk}(\lambda)}{\lambda}x} dx \quad (5)$$

where I_o is the IR intensity at the outermost surface, d is the alteration layer thickness, $\alpha_{AL}(\lambda)$ and $\alpha_{bulk}(\lambda)$ are the absorptivity of the alteration layer and the pristine bulk, respectively. Note that although the alteration layer was fitted with multiple sub-layers with varying solid fractions and thicknesses in the SE analysis, one sub-layer is usually dominant.[7, 50] For that reason, the contribution from the entire layer could be modeled with one effective $\alpha_{AL}(\lambda)$ and the total thickness d of the alteration layer; otherwise, too many unknown variables would be involved when the purpose of calculation is a simple approximation. After subtracting I_{bulk} from $I_{measured}$, the alteration layer contribution (I_{AL}) can be baseline-corrected using the asymmetric least squares method for further comparison.[51]

2.3. Attenuated total internal reflection infrared (ATR-IR) spectroscopy

The hydrous species (H_2O and Si-OH) in the alteration layer was measured using ATR-IR spectroscopy. The analysis was conducted using a Vertex 80 FT-IR spectrometer equipped with a single reflection ATR accessory (DiaMaxATR, Harrick Scientific Products) which has a diamond crystal. The incident angle of the IR beam at the crystal/sample interface was 45°. Each spectrum comprised an average of 100 scans with a resolution of 4 cm^{-1}. A spectrum of the crystal/air interface was used as the reference.

2.4. Spectroscopic ellipsometry

A spectroscopic ellipsometer (Alpha-SE, J.A. Woollam Co.) equipped with a light source covering the UV-Vis-NIR wavelength range of 381–893 nm at an incident angle of 70° was used to determine the thickness and porosity of alteration layers on corroded ISG samples. The thickness and porosity of the alteration layer were determined from measurements at ~50% relative humidity (RH). At this RH condition, a previous study found that ~75% of the accessible internal pores are filled with molecular water.[7] In the SE analysis, the alteration layer was modeled with multiple sub-layers using the Bruggeman effective medium approximation (EMA) composed of three

phases: solid, water, and void. The optical properties of the solid phase were assumed to be the same as the pristine ISG due to the difficulty in independently determining the optical properties of the solid phase of a porous solid.[7] In modeling the ellipsometric data, the pore-volume fraction filled with water at ~50%RH was assumed constant at 75%, relative to the accessible internal dry pore volume determined at 0% RH.[7]

In addition to the SE data in the UV-Vis-NIR range, spectroscopic ellipsometry data in the mid-IR range was also collected using an IR-VASE instrument (IR-VASE, J.A. Woollam Co.) equipped with a DTGS detector (working range 250 – 8000 cm^{-1}). The spectra of the uncorroded and corroded ISG specimens were collected at 50° and 55° incident angles with 16 cm^{-1} resolution. Optical constants in the IR wavelength range for bulk ISG were determined using a generalized oscillator (GenOsc) model comprising a host of Gaussian (G) and Gaussian-Lorentzian (G-L) oscillators. Results were very comparable to those obtained in a previous work.[46] These optical constants for the bulk were fixed in subsequent analysis of the alteration layer. Notably, the longer wavelength range associated with mid-IR frequencies generally leads to the lower sensitivity to relatively-thin, low-index-contrast surface layers in the (mostly) transparent range from 2000-6000 cm^{-1}. As such, there were limited oscillatory features useful for independent fitting of layer thicknesses. For that reason, the layer thickness was fixed to the value obtained from SE analysis in the UV-Vis-NIR range where such sensitivity is improved. The absorbing region of the IR spectra (<2000 cm^{-1}) for the alteration layer could then be modeled as a single-layer using an independent GenOsc model with a similar set of G and G-L oscillators for the glass network structure, along with new oscillators at higher frequencies representing bending and stretching vibrations from H_2O and OH evident in the IR-VASE spectra. Once the complex refractive index ($n(\lambda) + ik(\lambda)$) is determined for the alteration layer and the pristine bulk, then it is possible to theoretically calculate the SR-IR spectrum of a corroded sample with a given thickness (d) using the Fresnel coefficients to compare with the experimentally measured spectrum, $I_{measured}(\omega)$.

3. Results and Discussion

3.1. Effects of the presence of exogenous cation in the solution on alteration layer thickness on ISG corroded at pH 7, 90°C

The ISG samples in this study were corroded in aqueous solutions initially saturated with respect to amorphous silica.[40] Under this condition, the formation of alteration layers is expected mainly due to the preferential dissolution of Na and B (and Ca as well to a certain extent) from the glass and release into the aqueous solution; at the same time, proton and water ingress into the nano-porous alteration layer and glass network can undergo restructuring.[8, 16, 40, 52-54] The leaching of these elements from the glass was found to follow a monotonous square-root-of-time dependency which suggests that the release of these elements is controlled by diffusion.[9, 52, 55, 56] Thus, the evolution of the alternation layer thickness can be modeled according to Fick's second law.[8]

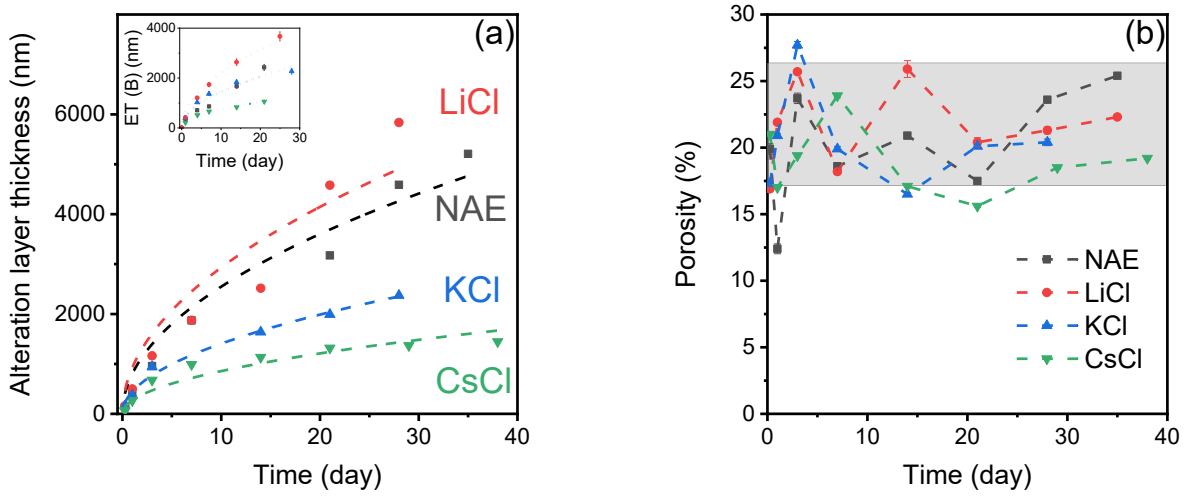

Figure 2. (a) Thicknesses of alteration layers formed on polished ISG glass surfaces corroded in different electrolyte conditions determined using SE. The trend lines are fits of alteration layer thicknesses using a $t^{1/2}$ dependence. Inset is the data taken from the paper by Collin et al. in which corrosion of crushed fine powders was studied and the alteration layer thickness was estimated from the mass balance of boron (B) species measured in the solution phase.[9] (b) Porosity of the thickest sublayer of alteration layer determined with SE. Here the porosity is the sum of the void and water-filled fraction. The error bar from the model fit is smaller than the size of symbols in many cases. NAE stands for 'no added electrolyte'.

The SE-determined thicknesses of alteration layers formed on corroded ISG samples are given in Figure 2a, as a function of corrosion time (t). The $\sqrt{t}$ dependence of the alteration layer thicknesses shown in Figure 2a suggests that under the silica saturated conditions of this study, the release of soluble species from ISG is diffusion-controlled. This is in good agreement with the results reported in the literature.[9] The inset displays the equivalent thickness (ET) of alteration layers on ISG powders corroded under the same experimental conditions, as determined by the mass balance of boron (B) species dissolved into the solution.[9] The thicknesses from two studies are not exactly the same due to the use of different techniques in thickness calculations and the form of samples used in the corrosion experiments (flat coupons in the current study, versus crushed powders in the reference).[13, 34, 35] Nonetheless, the results of both studies show that the alteration layer thickness is the highest on ISG samples corroded in solutions containing LiCl, and is the lowest in the one containing CsCl.

The overall porosity of the alteration layers formed on ISG samples corroded in different electrolyte conditions are given in Figure 2b. The results reveal that the alteration layers are highly porous with a porosity range of roughly 17~27% depending on corrosion time and condition. Note that the assumptions made in the ellipsometry analysis (detailed in section 2.4) limit the accuracy of the total porosity estimation. It has been shown previously that, for this relatively short corrosion time, most pores that are accessible by water molecules are less than 2 nm in diameter.[7, 8, 40] The porosity values in the current study are comparable to those estimated from thermogravimetric analysis (TGA) of ISG powders corroded under the same conditions.[9] The TGA results show that, for ISG powders corroded for about 30 days in NAE, LiCl KCl, CsCl electrolyte solutions, the porosity values of alteration layers were ~28 ± 5%, 28 ± 5%, 22 ± 4%, and 16 ± 3%, respectively.[9]

The diffusivity of reactants and corrosion products through the alteration layer may be expected to be governed by the porosity; if so, one may expect to see a correlation between the porosity and the diffusivity. The dependence of the corrosion rate of ISG on the identity of the electrolytes present in solution was indeed previously attributed to the mismatch between the size of the sodium ions leaching from the glass versus that of the exogenous cations diffusing into the alteration layer, which could ostensibly affect ion exchange behavior.[9] However, the transport behavior of these ions, as well as their hydration structures, could be also affected by the nano-

confined geometry inside the porous network.[9] Furthermore, the pore size distribution as well as their connectivity plays critical roles in determining the overall diffusivity. Without knowing such details, it would be difficult to predict whether there should be a direct correlation between the alteration layer growth kinetics and the porosity or not.

3.2. Effects of exogenous cations on hydrous species in alteration layer of ISG corroded at pH 7, 90°C

The chemical durability of glass can be significantly affected by the presence of hydrous species within the silicate network (H_2O and Si-OH).[57] In this study, hydrous species in the alteration layer were investigated using ATR-IR spectroscopy. The H_2O bending band (~1630 cm^{-1}) and OH stretching band (2800 – 3800 cm^{-1}) of ISG samples corroded in NAE, LiCl and KCl conditions for 3 days and in CsCl condition for 7 days are shown in Figure 3a. The sample corroded in the solution containing CsCl for 7 days was chosen for comparison because its alteration layer thickness was closer to the thicknesses of samples corroded in other conditions for 3 days (Figure 2a). The intensity of the water bending band at ~1630 cm^{-1} must correlate with the concentration of molecular water in the alteration layer, while the OH stretching band arises from a convolution of both molecular water in the nano-pores (Figure 2b) and silanol groups (Si-OH) in the alteration layer.[58] Water molecules in the porous altered layer can have hydrogen bond (HB) distributions that are different from those in bulk liquid under equilibrium conditions.[50] Results from molecular dynamics simulations of HBs of hydrous species in nano-porous gels of aluminosilicate glass showed that the two most abundant types are HBs between water molecules and HBs between the OH of silanol groups and the oxygen of water.[50] The HBs between OH of silanol and oxygen of siloxane groups (Si-O-Si) are also probable, and may vary depending on the nanopore size. All HB types studied have broad O···H distance distributions and their spectral bands overlap significantly; thus, the deconvolution of the measured spectrum into contributing components is difficult.[50, 59]

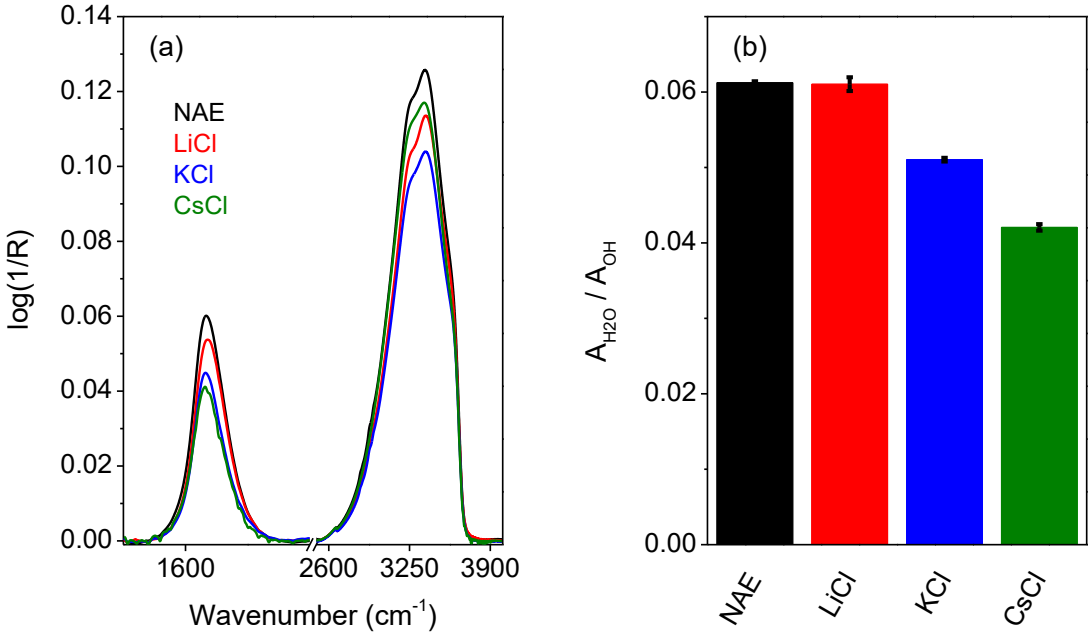

Figure 3. (a) ATR-IR spectra of the ISG samples corroded in NAE, LiCl and KCl conditions for 3 days and in CsCl condition for 7 days. These samples have comparable alteration layer thicknesses (~1000 nm). (b) Integrated area ratios of the water bending band (~1630 cm^{-1}) to the OH stretching band (~2800-3800 cm^{-1}). The error bars show standard error of 3 measurements.

A direct comparison of the absolute intensity of the ATR-IR spectra of ISG samples corroded in different electrolyte conditions is not possible, because the ATR-IR intensity is highly sensitive to intimacy of the contact between the sample surface and the ATR crystal. Any air gap between the sample surface and the ATR crystal due to surface roughness could decrease the observed IR intensity. Nonetheless, it is still possible to compare the integrated area ratios of the water bending and the OH stretching bands (A_{H2O}/A_{OH}) of each spectrum (Figure 3b). A higher area value means the molecular water fraction among the hydrous species is higher compared to the case with a lower value.

The integrated area ratios shown in Figure 3b suggest that the alteration layers formed in the NAE and LiCl conditions have a higher fraction of molecular water compared to the samples corroded in the KCl and CsCl conditions, and this is consistent with values reported in the literature.[9] It is difficult to attribute this difference solely to the difference in porosity of alteration layers among the samples due to experimental uncertainty in measuring the porosity (Figure 2b).[9] Another possibility that must be considered is the reorganization of the Si-O-Si and

Si-O-Al network, which can continuously occur upon the loss of network modifiers (sodium and calcium ions) and the network formers (boron species) during the corrosion process; such restructuring can affect the pore connectivity within the alteration layer.[41] Current experimental findings are not sufficient to determine the dominant mechanism that leads to the difference in the integrated area ratios. The glass network reorganization may also affect the transport of chemical species leaching from the alteration layer, as well as protons, exogenous cations, and water molecules diffusing into the alteration layer. If the proton (H^+) diffuses as a hydronium (H_3O^+) ion, the effective diffusivity of protons and molecular water could be similar. But, if H^+ diffuses by itself (i.e., through ion exchange only with Na^+), then its diffusivity could be faster than the diffusivity of molecular water (which would require larger open spaces within the network). Experimentally, it has been shown that the proton and water diffusion rates can differ from each other and vary over time during the acid leaching of soda lime silicate glass.[58] In a study with porous Vycor glass, it was reported that the co-presence of $CaCl_2$ with water can significantly reduce the local diffusion coefficient of confined water compared to pure water in the same material.[60] If the proton and water diffusivities are affected to different extents by the presence of exogenous ions, then it could explain (or at least partially contribute to) different relative abundances of SiOH and H_2O in the alteration layers of these samples corroded in the presence of different electrolytes in the solution.

3.3. Vibrational spectroscopy analysis of the alteration layer network structure

Previous work on the effect of exogeneous cations on glass corrosion investigated the alteration layer network structure by means of NMR probing the first-shell coordination (Q_n speciation) of silicon atoms.[9] The longer-range connectivity of those species consisting the entire network could be inferred from vibrational spectroscopy analysis because vibrational spectral features of amorphous solids are sensitive to the distribution of short- and medium-range orders of chemical bonds.[61-65] In the case of silica glass, the IR spectrum has been shown to be sensitive to small differences in the glass network structure[61, 62, 66] that can be correlated to differences in properties.[67] Especially, the peak position of the Si-O network stretch mode around 1050-1120 cm^{-1} in IR appears to be highly sensitive to minute changes in the bond length distribution of chemical bonds constituting the glass network.[61, 62, 68] The vibrational spectrum of the thin alteration layer on a monolithic flat sample surface can be obtained using either IR-

VASE or SR-IR. IR-VASE can give full spectral information,[69] but it may not be readily available in many laboratories. SR-IR is readily available in most experimental laboratories, but the spectrum is often convoluted with the contributions from the bulk. In this section, we discuss the use of these two techniques and make qualitative comparison of the information that can be obtained from the two methods.

3.3.1. Complex refractive index of the alteration layer determined with IR-VASE

IR-VASE was used to determine the complex refractive index, $n + ik$, of the alteration layer formed on ISG sample corroded for 34 days in KCl condition as well as the pristine ISG glass. The raw data of measured ellipsometric angles Ψ and Δ in the 254-5955 cm^{-1} region are shown in Figure S1 in the SI and the real and imaginary parts of the refractive index obtained from the optical model fits are shown in Figure 4. Since the imaginary part of the refractive index is closely related to the absorption spectrum, the discussion will be focused on this part. In the k-spectrum of the pristine, two bands are clearly noticed. The large band centered at ~1026 cm^{-1} is ascribed to the Si-O-(Si, Al, B) stretch mode and the small one centered at ~1400 cm^{-1} is the B-O stretch in the glass network.[45, 70, 71] In the k-spectrum of the alteration layer, the B-O stretch mode is completely gone because the boron species are all leached out in the alteration layer.[8] It is also noted that the Si-O stretch band is blue-shifted to ~1057 cm^{-1} and its band width is narrower. The shoulder peak at ~1200 cm^{-1} as well two minor peaks at 780 cm^{-1} and ~900 cm^{-1} become more prominent in the alteration layer spectrum.

The blue shift of the Si-O band and the growth of the 1200 cm^{-1} shoulder have conventionally been interpreted as an indication of the transition to “more silica-like” network structure.[62, 72, 73] This interpretation is congruent with the compositional change – the loss of modifier ions as well boron species from the glass network. In recent MD simulation studies for silica and sodium silicate glasses, the intensity-weighted average peak position was found to correlate with the Si-O bond length distribution; as the bond length gets shorter by 0.01 Å, the stretch band position increases by ~45 cm^{-1}.[61, 62, 68, 74, 75] If the same is applicable to the alteration layer spectrum, then the blue-shift by ~31 cm^{-1} seen in Figure 4 may imply that the loss of modifier ions and boron species is accompanied by the decrease in the average Si-O bond length by ~0.007 Å. The water content in the porous glass can shift the Si-O absorption band position by 1~2 cm^{-1} in the SR-IR measurement due to a change in the effective refractive index;[76] but the

observed shift in Figure 4 is much larger than the optical artifact originating from simple pore filling. Since the Si-O bond is extremely stiff (with a force constant of ~5 mdyne/Å),[74] even a small degree of strain in the bond length distribution could add up to a large internal stress as the alteration layer thickness increases, which could be a driving force for structural reorganization.[77, 78] If the peak width is to reflect the distribution of the bond length, it appears that the Si-O bond length distribution is narrower for the alteration layer than the pristine glass. The longer bond length side of the distribution (which is the lower wavenumber side of the peak) is significantly reduced compared to the shorter bond length side (higher wavenumber side); this change is associated with the extraction of all sodium and part of calcium modifier ions as well as boron from the glass network. Further details shall require advanced and systematic computational approaches, which are beyond the scope of the current study and would be a subject for future work.

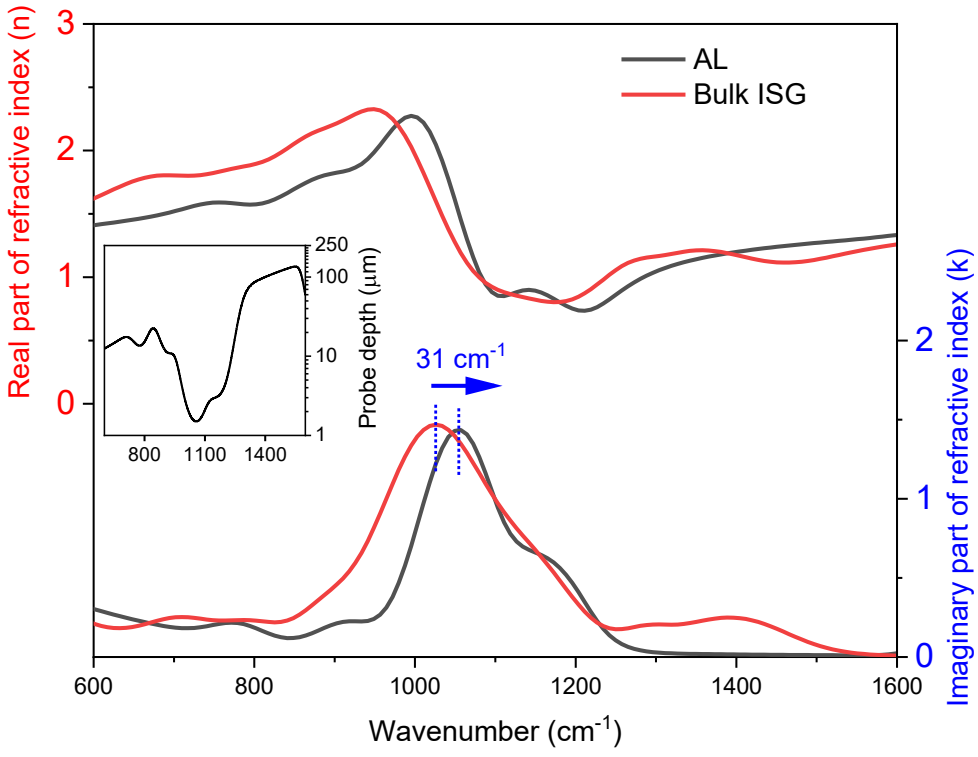

Figure 4. Complex refractive index, $n + ik$, of pristine bulk ISG (red lines) and the alteration layer (AL, black lines) obtained from IR-VASE analysis of ISG sample corroded in the 13 mM KCl condition for 34 days. The thickness of the alteration layer was pre-determined using the SE data in the UV-Vis-NIR region (see text). The inset shows the effective probe depth ($3\times d_p$) calculated using the refractive index of the alteration layer.

3.3.2. SR-IR analysis of the alteration layer formed on ISG upon aqueous corrosion

SR-IR analysis can be carried out easily on any FT-IR instrument by adding a simple reflection accessory and the data collection is very easy. Nonetheless, its use is quite limited due to the difficulty of deconvoluting spectral features of the surface layer from the bulk when the surface layer is thinner than the probe depth of SR-IR. The inset in Figure 4 plots the effective probe depth as a function of IR wavenumber calculated using the refractive index of the alteration layer determined with IR-VASE. At the maximum intensity position of the Si-O stretch band, the effective probe depth is on the order of 1 μm. However, in other spectral regions, it readily exceeds 10 μm, resulting in substantial contributions from the bulk glass. Moreover, aqueous corrosion often produces layers with inhomogeneous distributions of porosity and composition along the depth axis.[7] In this study, we propose a simple approximation model (equations 2 – 5) based on the IR intensity attenuation inside the sample to subtract the bulk contribution and extract the spectral features more relevant to the alteration layer. In this approximation, the difference in the real part (n) of refractive index between the alteration layer and the bulk is assumed to be negligible, although the IR-VASE analysis shows some differences as shown in Figure 4. Similar to IR-VASE analysis, small degrees of compositional and porosity variations are ignored and the entire alteration layer is assumed homogeneous for the sake of simplicity.[7]

The SR-IR spectra of ISG samples corroded in NAE, LiCl and KCl conditions for 3 days and in CsCl condition for 7 days, which all have roughly 1 μm thickness of alteration layers (Figure 2a), are shown in Figure 5a. The full data sets are provided in Figure S2 in the SI. All spectra of the corroded samples show a blue-shift of ~33 cm^{-1} in the maximum intensity position of the Si-O stretch band, which is consistent with the IR-VASE data found for the alteration layer formed by corrosion in the KCl condition for 34 days (Figure 4). The ISG sample corroded in the LiCl condition has a lower measured intensity compared to the samples corroded in other conditions; this could be due to more scattering of the probe beam than other samples due to small variations in surface roughness. Thus, the absolute intensity among the samples could not be compared. Nonetheless, the peak position and shape of each spectrum can still be usefully compared if the bulk contribution is subtracted using equations 2 – 5, with the layer thickness determined from the SE analysis (Figure 2a), and the resulting spectra each baseline-corrected and then normalized to the same scale.

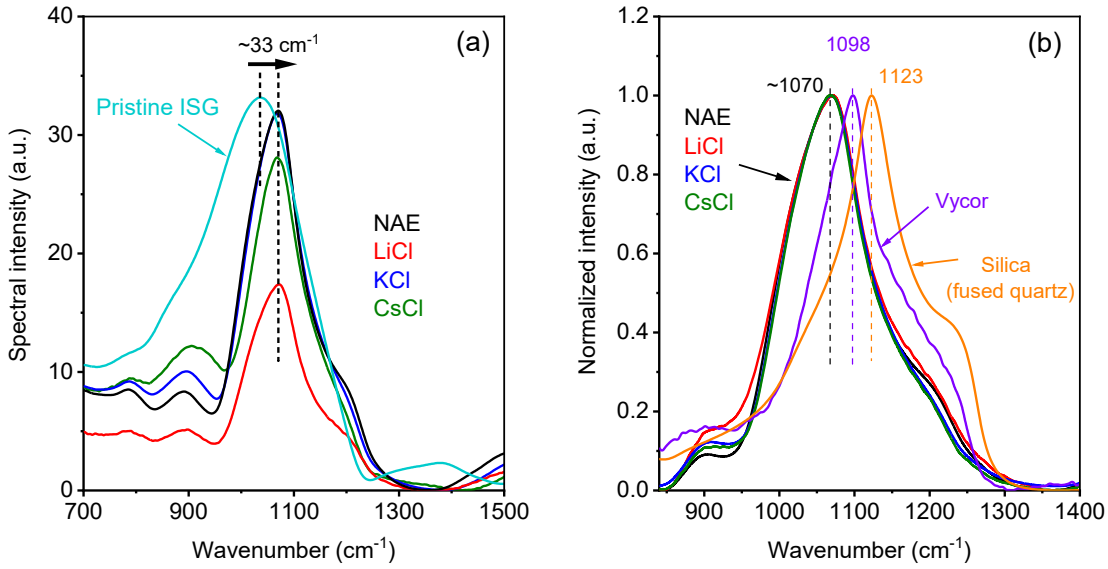

Figure 5. (a) SR-IR spectra of pristine ISG and ISG samples corroded in NAE, LiCl and KCl conditions for 3 days and in CsCl condition for 7 days with comparable alteration layer thicknesses (~1000 nm). (b) IR spectra after bulk contribution subtraction and normalization of IR spectra in (a). The IR spectra of Vycor and silica (fused quartz) are given for comparison.

In Figure 5b, the processed spectra of the alteration layers produced in different electrolyte conditions are compared. They are almost identical to each other. For comparison, the SR-IR spectra of unconsolidated Vycor (used as a model system for silica-rich porous glass) and fused quartz (used to represent pure silica) samples are also shown in Figure 5b.[79] The overall spectral shape of the processed data are much closer to those of Vycor and fused quartz than the pristine IGS spectrum shown in Figure 5a. The fact that the overall vibrational spectral features become closer to more resistant silica glass could be a reason that the remaining glass network is resistant to further hydrolysis. If so, the decrease in corrosion rate may not be totally irrelevant to this structural transition of the network. Again, if the correlation between the Si-O stretch band and the Si-O bond length distribution found for the silica and sodium silicate glasses is employed here,[61, 62, 68] then the large decrease in the lower wavenumber side of the Si-O stretch band upon corrosion (as shown in Figure 5a) could mean that the longer Si-O bonds in the glass network are more susceptible to the hydrolysis reaction; this may result in a net increase in the population of the Si-O bond lengths closer to the chemically more stable value (which would be the length of the Si-O bond in the silica glass produced thermally). Note that due to the non-equilibrium nature,

the glass with the same chemical composition can adopt drastically different network structure depending on the history of the sample.[80] In addition to the effect of glass network chemical composition (silica-like), local conditions within the alteration layer and outermost glass surface such as corrosion product concentration, pH, electrolytes, water structure could also contribute to the change of glass corrosion with time.[81]

3.3.3. Comparison of experimental SR-IR spectra and theoretically calculated SR-IR spectra

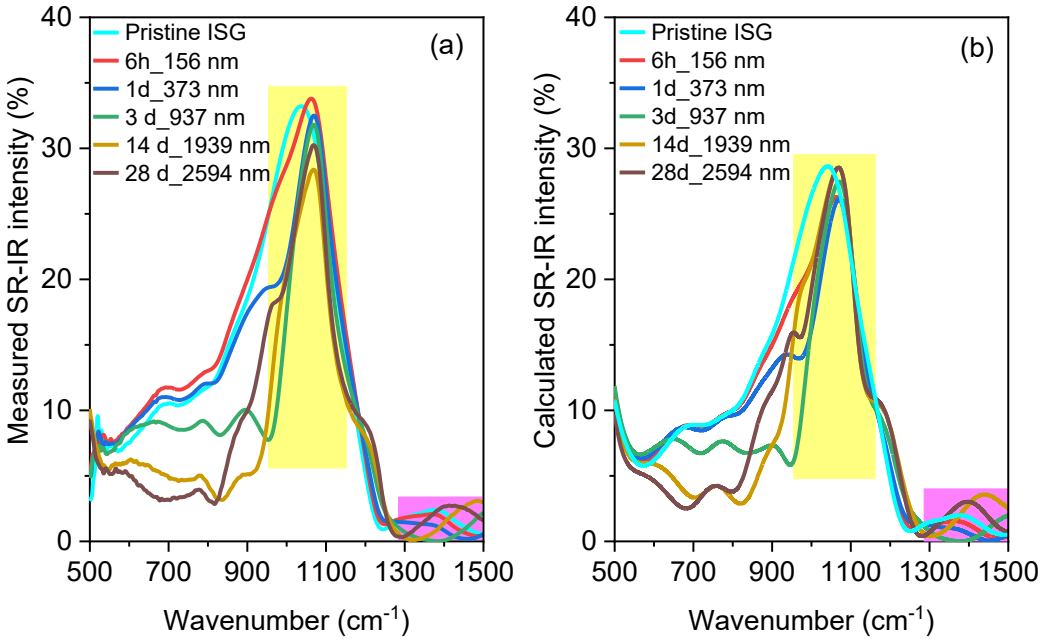

Figure 6. (a) Experimental SR-IR spectra of the ISG samples corroded in the KCl condition. (b) SR-IR spectra calculated using an optical model consisting of air, alteration layer and pristine ISG; the alteration layer thicknesses are the same to those of the ISG samples corroded in the KCl condition displayed in (a).

The experimentally measured SR-IR spectra can be compared with the simulated SR-IR spectra calculated theoretically using the thickness of the alteration layer determined from the SE analysis (shown in Figure 2a) and assuming that the refractive index of all alteration layers is the same as the one determined from the IR-VASE analysis of the ISG sample corroded in the KCl condition for 34 days (shown in Figure 4). The theoretical calculation details are given in the last section of the supporting information.[82] Again, the alteration layer can be assumed to have a uniform effective refractive index throughout the entire thickness for the simplicity. Figure 6

compares the experimental SR-IR spectra (Figure 6a) and the calculated spectra (Figure 6b) for the alteration layers with varying corrosion times. Although the absolute intensities are somewhat different, the overall peak shapes are in qualitative agreement. The discrepancy is attributed to the over-simplification of the heterogeneous alteration layer by modeling with a single homogeneous layer. Even with this potential error, it is noticeable that the peak shape of the main Si-O stretch mode region (950 – 1150 cm^{-1}) is remarkably similar to each other. This is because the effective probe depth in this spectral region is quite shallow (see the inset in Figure 4), thus the spectral feature is mostly dominated by the alteration layer. This also supports the efficacy of the simple approximation method used for the SR-IR data processing in Figure 5b.

It is interesting to note that the intensity of the B-O absorption band around ~1400 cm^{-1} decreases at the beginning of corrosion and then grows back in the 28-day spectrum in the experimental spectra (Figure 6a). Without the theoretical calculation, one could have interpreted it as the re-population of the boron species in the alteration layer around 28 days of corrosion. But, from the SIMS depth profiling analysis, it is well known that all boron species are dissolved out of the alteration layer.[40] In the theoretical calculation using the refractive index of the alteration layer that does not have the absorption band around 1400 cm^{-1} (Figure 4b), the same trend is observed (Figure 6b). This means that the re-appearance of the ~1400 cm^{-1} band in the SR-IR spectra originates from the optical artifact of probing the B-O stretching mode of the pristine bulk through the alteration layer with certain thickness that causes constructive interference in the detected reflection signal.

4. Conclusions

Evidenced by the thickness of alteration layers formed, LiCl enhances, and KCl and CsCl obstruct aqueous glass corrosion when they are exogenously-added. Hydrous species and the network structure of alteration layers of ISG samples corroded in aqueous solutions with exogenously-added LiCl, KCl and CsCl were investigated with infrared spectroscopy. ATR-IR spectroscopy revealed a lower ratio of molecular water over the surface-bound hydroxyl species in the KCl and CsCl conditions corresponding to more passivating altered layers than those of in LiCl and NAE conditions. A method to estimate the spectral features of the corroded glass from a

measured SR-IR spectrum of corroded glass surfaces was proposed. Analysis of the ISG samples corroded with the proposed method revealed no significant difference among the IR vibrational features, suggesting presence of similar glass network structures. The difference in the relative abundance of hydrous species in the alteration layers could be linked to the difference in the corrosion rates.

Acknowledgements. This work was supported as part of the Center for Performance and Design of Nuclear Waste Forms and Containers, an Energy Frontier Research Center funded by the U.S. Department of Energy, Office of Science, Basic Energy Sciences under Award # DE-SC0016584. The authors thank Prof. Michael A. Hickner (The Pennsylvania State University) for allowing the access to the spectroscopic ellipsometry setup in his lab.

References

[1] J. Neeway, A. Abdelouas, B. Grambow, S. Schumacher, Dissolution mechanism of the SON68 reference nuclear waste glass: New data in dynamic system in silica saturation conditions, Journal of Nuclear Materials, 415 (2011) 31-37.
[2] S. Gin, X. Beaudoux, F. Angéli, C. Jégou, N. Godon, Effect of composition on the short-term and long-term dissolution rates of ten borosilicate glasses of increasing complexity from 3 to 30 oxides, Journal of Non-Crystalline Solids, 358 (2012) 2559-2570.
[3] S. Gin, A. Abdelouas, L.J. Criscenti, W.L. Ebert, K. Ferrand, T. Geisler, M.T. Harrison, Y. Inagaki, S. Mitsui, K.T. Mueller, J.C. Marra, C.G. Pantano, E.M. Pierce, J.V. Ryan, J.M. Schofield, C.I. Steefel, J.D. Vienna, An international initiative on long-term behavior of high-level nuclear waste glass, Materials Today, 16 (2013) 243-248.
[4] J.D. Vienna, J.V. Ryan, S. Gin, Y. Inagaki, Current Understanding and Remaining Challenges in Modeling Long-Term Degradation of Borosilicate Nuclear Waste Glasses, International Journal of Applied Glass Science, 4 (2013) 283-294.
[5] G.S. Frankel, J.D. Vienna, J. Lian, J.R. Scully, S. Gin, J.V. Ryan, J. Wang, S.H. Kim, W. Windl, J. Du, A comparative review of the aqueous corrosion of glasses, crystalline ceramics, and metals, npj Materials Degradation, 2 (2018).
[6] D.E. Perea, D.K. Schreiber, J.V. Ryan, M.G. Wirth, L. Deng, X. Lu, J. Du, J.D. Vienna, Tomographic mapping of the nanoscale water-filled pore structure in corroded borosilicate glass, npj Materials Degradation, 4 (2020) 8.
[7] D. Ngo, H. Liu, N. Sheth, R. Lopez-Hallman, N.J. Podraza, M. Collin, S. Gin, S.H. Kim, Spectroscopic ellipsometry study of thickness and porosity of the alteration layer formed on

international simple glass surface in aqueous corrosion conditions, npj Materials Degradation, 2 (2018) 20.
[8] M. Collin, M. Fournier, P. Frugier, T. Charpentier, M. Moskura, L. Deng, M. Ren, J. Du, S. Gin, Structure of International Simple Glass and properties of passivating layer formed in circumneutral pH conditions, npj Materials Degradation, 2 (2018) 4.
[9] M. Collin, M. Fournier, T. Charpentier, M. Moskura, S. Gin, Impact of alkali on the passivation of silicate glass, npj Materials Degradation, 2 (2018) 16.
[10] S. Gin, A.H. Mir, A. Jan, J.M. Delaye, E. Chauvet, Y. De Puydt, A. Gourgiotis, S. Kerisit, A General Mechanism for Gel Layer Formation on Borosilicate Glass under Aqueous Corrosion, The Journal of Physical Chemistry C, 124 (2020) 5132-5144.
[11] J.D. Vienna, J.J. Neeway, J.V. Ryan, S.N. Kerisit, Impacts of glass composition, pH, and temperature on glass forward dissolution rate, npj Materials Degradation, 2 (2018).
[12] M.I. Ojovan, W.E. Lee, Glassy Wasteforms for Nuclear Waste Immobilization, Metallurgical and Materials Transactions A, 42 (2010) 837-851.
[13] H. Liu, D. Ngo, M. Ren, J. Du, S.H. Kim, Effects of surface initial condition on aqueous corrosion of glass-A study with a model nuclear waste glass, Journal of the American Ceramic Society, 102 (2019) 1652-1664.
[14] F. Angeli, T. Charpentier, P. Jollivet, D. de Ligny, M. Bergler, A. Veber, S. Gin, H. Li, Effect of thermally induced structural disorder on the chemical durability of International Simple Glass, npj Materials Degradation, 2 (2018).
[15] X. Guo, S. Gin, H. Liu, D. Ngo, J. Luo, S.H. Kim, C. Mohanty, J.D. Vienna, J.V. Ryan, G.S. Frankel, Near-field corrosion interactions between glass and corrosion resistant alloys, npj Materials Degradation, 4 (2020) 10.
[16] S. Gin, P. Jollivet, M. Fournier, C. Berthon, Z. Wang, A. Mitroshkov, Z. Zhu, J.V. Ryan, The fate of silicon during glass corrosion under alkaline conditions: A mechanistic and kinetic study with the International Simple Glass, Geochimica et Cosmochimica Acta, 151 (2015) 68-85.
[17] P. Jollivet, S. Gin, S. Schumacher, Forward dissolution rate of silicate glasses of nuclear interest in clay-equilibrated groundwater, Chemical Geology, 330-331 (2012) 207-217.
[18] P.M. Dove, The dissolution kinetics of quartz in aqueous mixed cation solutions, Geochimica et Cosmochimica Acta, 63 (1999) 3715-3727.
[19] P.M. Dove, C.J. Nix, The influence of the alkaline earth cations, magnesium, calcium, and barium on the dissolution kinetics of quartz, Geochimica et Cosmochimica Acta, 61 (1997) 3329-3340.
[20] P.M. Dove, D.A. Crerar, Kinetics of quartz dissolution in electrolyte solutions using a hydrothermal mixed flow reactor, Geochimica et Cosmochimica Acta, 54 (1990) 955-969.
[21] L.-S. Du, J.F. Stebbins, Network connectivity in aluminoborosilicate glasses: A high-resolution 11B, 27Al and 17O NMR study, Journal of Non-Crystalline Solids, 351 (2005) 3508-3520.
[22] R.L. Mozzi, B.E. Warren, The structure of vitreous silica, Journal of Applied Crystallography, 2 (1969) 164-172.
[23] A.C. Wright, Neutron scattering from vitreous silica. V. The structure of vitreous silica: What have we learned from 60 years of diffraction studies?, Journal of Non-Crystalline Solids, 179 (1994) 84-115.
[24] B.E. Warren, J. Biscoe, Fourier analysis of X-ray patterns of soda-silica glass, Journal of the American Ceramic Society, 21 (1938) 259-265.

[25] B.E. Warren, X-ray Diffraction Study of the Structure of Glass, Chemical Reviews, 26 (1940) 237-255.
[26] W.R. Taylor, Application of infrared spectroscopy to studies of silicate glass structure: Examples from the melilite glasses and the systems Na2O-SiO2 and Na2O-Al2O3-SiO2, Proceedings of the Indian Academy of Sciences - Earth and Planetary Sciences, 99 (1990) 99-117.
[27] D.M. Sanders, W.B. Person, L.L. Hench, Quantitative Analysis of Glass Structure with the Use of Infrared Reflection Spectra, Appl. Spectrosc., 28 (1974) 247-255.
[28] W.B. White, D.G. Minser, Raman spectra and structure of natural glasses, Journal of Non-Crystalline Solids, 67 (1984) 45-59.
[29] H. Eckert, Advanced Dipolar Solid State Nmr Spectroscopy of Glasses, in: M. Affatigato (Ed.) Modern Glass Characterization, 2015, pp. 1-46.
[30] P.J. Bray, Nuclear magnetic resonance studies of glass structure, Journal of Non-Crystalline Solids, 73 (1985) 19-45.
[31] H. Eckert, Spying with spins on messy materials: 60 Years of glass structure elucidation by NMR spectroscopy, International Journal of Applied Glass Science, 9 (2018) 167-187.
[32] F. Pfeiffer, W. Zhang, I.K. Robinson, Coherent grazing exit x-ray scattering geometry for probing the structure of thin films, Applied Physics Letters, 84 (2004) 1847-1849.
[33] R.A. Fry, N. Tsomaia, C.G. Pantano, K.T. Mueller, 19F MAS NMR Quantification of Accessible Hydroxyl Sites on Fiberglass Surfaces, Journal of the American Chemical Society, 125 (2003) 2378-2379.
[34] H. He, S.H. Hahn, J. Yu, Q. Qiao, A.C.T. van Duin, S.H. Kim, Friction-induced subsurface densification of glass at contact stress far below indentation damage threshold, Acta Materialia, 189 (2020) 166-173.
[35] H. He, Q. Qiao, J. Yu, S.H. Kim, Synergy between surface mechanochemistry and subsurface dissolution on wear of soda lime silica glass in basic solution, Journal of the American Ceramic Society, n/a (2020).
[36] G. Laroche, J. Fitremann, N. Gherardi, FTIR-ATR spectroscopy in thin film studies: The importance of sampling depth and deposition substrate, Applied Surface Science, 273 (2013) 632-637.
[37] D. Rébiscoul, F. Bruguier, V. Magnin, S. Gin, Impact of soda-lime borosilicate glass composition on water penetration and water structure at the first time of alteration, Journal of Non-Crystalline Solids, 358 (2012) 2951-2960.
[38] S.-i. Amma, J. Luo, C.G. Pantano, S.H. Kim, Specular reflectance (SR) and attenuated total reflectance (ATR) infrared (IR) spectroscopy of transparent flat glass surfaces: A case study for soda lime float glass, Journal of Non-Crystalline Solids, 428 (2015) 189-196.
[39] F. Geotti-Bianchini, M. Preo, M. Guglielmi, C.G. Pantano, Infrared reflectance spectra of semi-transparent SiO2 rich films on silicate glasses: influence of the substrate and film thickness, Journal of Non-Crystalline Solids, 321 (2003) 110-119.
[40] S. Gin, P. Jollivet, M. Fournier, F. Angeli, P. Frugier, T. Charpentier, Origin and consequences of silicate glass passivation by surface layers, Nature Communications, 6 (2015) 6360.
[41] S. Gin, M. Collin, P. Jollivet, M. Fournier, Y. Minet, L. Dupuy, T. Mahadevan, S. Kerisit, J. Du, Dynamics of self-reorganization explains passivation of silicate glasses, Nature Communications, 9 (2018) 2169.

[42] D.A. Castilla-Casadiego, L. Pinzon-Herrera, M. Perez-Perez, B.A. Quiñones-Colón, D. Suleiman, J. Almodovar, Simultaneous characterization of physical, chemical, and thermal properties of polymeric multilayers using infrared spectroscopic ellipsometry, Colloids Surf A Physicochem Eng Asp, 553 (2018) 155-168.
[43] N.-N. Wei, Z. Yang, H.-B. Pan, F. Zhang, Y.-X. Liu, R.-P. Wang, X. Shen, S.-X. Dai, Q.-H. Nie, Variable angle spectroscopic ellipsometry and its applications in determining optical constants of chalcogenide glasses in infrared, Chinese Physics B, 27 (2018).
[44] T. Lombardo, C. Loisel, L. Gentaz, A. Chabas, M. Verita, I. Pallot-Frossard, Long term assessment of atmospheric decay of stained glass windows, Corrosion Engineering, Science and Technology, 45 (2010) 420-424.
[45] J. Luo, N.J. Smith, C.G. Pantano, S.H. Kim, Complex refractive index of silica, silicate, borosilicate, and boroaluminosilicate glasses – Analysis of glass network vibration modes with specular-reflection IR spectroscopy, Journal of Non-Crystalline Solids, 494 (2018) 94-103.
[46] T.C. Kaspar, J.V. Ryan, C.G. Pantano, J. Rice, C. Trivelpiece, N.C. Hyatt, C.L. Corkhill, C. Mann, R.J. Hand, M.A. Kirkham, C.L. Crawford, C.M. Jantzen, J. Du, X. Lu, M.T. Harrison, C. Cushman, M.R. Linford, N.J. Smith, Physical and optical properties of the International Simple Glass, npj Materials Degradation, 3 (2019) 15.
[47] R.A. Synowicki, Suppression of backside reflections from transparent substrates, physica status solidi c, 5 (2008) 1085-1088.
[48] P. Frugier, S. Gin, Y. Minet, T. Chave, B. Bonin, N. Godon, J.E. Lartigue, P. Jollivet, A. Ayral, L. De Windt, G. Santarini, SON68 nuclear glass dissolution kinetics: Current state of knowledge and basis of the new GRAAL model, Journal of Nuclear Materials, 380 (2008) 8-21.
[49] F. Geotti-Bianchini, L.D. Rui, M.G. G. Gagliardi, C.G. Pantano, New interpretation of the IR reflectance spectra of SiO2 rich films on soda lime glass, Glastechnische Berichte, 64 (1991) 205–217.
[50] D. Ngo, H. Liu, Z. Chen, H. Kaya, T.J. Zimudzi, S. Gin, T. Mahadevan, J. Du, S.H. Kim, Hydrogen bonding interactions of H2O and SiOH on a boroaluminosilicate glass corroded in aqueous solution, npj Materials Degradation, 4 (2020) 1.
[51] P.H.C. Eilers, H.F.M. Boelens, Baseline Correction with Asymmetric Least Squares Smoothing, in, Leiden University, 2005.
[52] C. Lenting, O. Plümper, M. Kilburn, P. Guagliardo, M. Klinkenberg, T. Geisler, Towards a unifying mechanistic model for silicate glass corrosion, npj Materials Degradation, 2 (2018) 28.
[53] S. Gin, P. Jollivet, G. Barba Rossa, M. Tribet, S. Mougnaud, M. Collin, M. Fournier, E. Cadel, M. Cabie, L. Dupuy, Atom-Probe Tomography, TEM and ToF-SIMS study of borosilicate glass alteration rim: A multiscale approach to investigating rate-limiting mechanisms, Geochimica et Cosmochimica Acta, 202 (2017) 57-76.
[54] C. Lenting, O. Plümper, M. Kilburn, P. Guagliardo, M. Klinkenberg, T. Geisler, Towards a unifying mechanistic model for silicate glass corrosion, npj Materials Degradation, 2 (2018).
[55] B. Grambow, Corrosion of Glass, in: R.W. Revie (Ed.) Uhlig's Corrosion Handbook, John Wiley & Sons, 2011, pp. 399-420.
[56] T. Chave, P. Frugier, A. Ayral, S. Gin, Solid state diffusion during nuclear glass residual alteration in solution, Journal of Nuclear Materials, 362 (2007) 466-473.
[57] M. Tomozawa, C.Y. Erwin, M. Takata, E.B. Watson, Effect of Water Content on the Chemical Durability of Na2O 3SiO2 Glass, Journal of the American Ceramic Society, 65 (1982) 182-183.

[58] J. Luo, S.-i. Amma, L. Chen, D. Ngo, J.C. Mauro, C.G. Pantano, S.H. Kim, Relative abundance of subsurface hydroxyl and molecular water species in silicate and aluminosilicate glasses, Journal of Non-Crystalline Solids, 510 (2019) 179-185.
[59] E. Balan, K. Refson, M. Blanchard, S. Delattre, M. Lazzeri, J. Ingrin, F. Mauri, K. Wright, B. Winkler, Theoretical infrared absorption coefficient of OH groups in minerals, American Mineralogist, 93 (2008) 950-953.
[60] E. Mamontov, D.R. Cole, Quasielastic neutron scattering study of dynamics of CaCl2 aqueous solution confined in Vycor glass, Physical Chemistry Chemical Physics, 8 (2006) 4908-4914.
[61] J. Luo, Y. Zhou, S.T. Milner, C.G. Pantano, S.H. Kim, Molecular dynamics study of correlations between IR peak position and bond parameters of silica and silicate glasses: Effects of temperature and stress, Journal of the American Ceramic Society, 101 (2018) 178-188.
[62] H. Liu, S.H. Hahn, M. Ren, M. Thiruvillamalai, T.M. Gross, J. Du, A.C.T. Duin, S.H. Kim, Searching for correlations between vibrational spectral features and structural parameters of silicate glass network, Journal of the American Ceramic Society, (2020).
[63] D. Tuschel, Why Are the Raman Spectra of Crystalline and Amorphous Solids Different, Spectroscopy, 32 (2017) 26–33.
[64] S.R. Elliott, Medium-range structural order in covalent amorphous solids, Nature, 354 (1991) 445-452.
[65] R. Zallen, The Physics of Amorphous Solids, WILEY-VCH Verlag GmbH & Co. KGaA, Weinheim, 1998.
[66] S.R. Ryu, M. Tomozawa, Fictive temperature measurement of amorphous SiO2 films by IR method, Journal of Non-Crystalline Solids, 352 (2006) 3929-3935.
[67] A. Agarwal, M. Tomozawa, Correlation of silica glass properties with the infrared spectra, Journal of Non-Crystalline Solids, 209 (1997) 166–174.
[68] J. Luo, Y. Zhou, C.G. Pantano, S.H. Kim, Correlation between IR peak position and bond parameter of silica glass: Molecular dynamics study on fictive temperature (cooling rate) effect, Journal of the American Ceramic Society, 101 (2018) 5419-5427.
[69] H.G. Tompkins, T. Tiwald, C. Bungay, A.E. Hooper, Use of Molecular Vibrations to Analyze Very Thin Films with Infrared Ellipsometry, The Journal of Physical Chemistry B, 108 (2004) 3777-3780.
[70] E.I. Kamitsos, Infrared Spectroscopy of Glasses, in: M. Affatigato (Ed.) Modern Glass Characterization, 2015, pp. 1-42.
[71] D. Möncke, M. Dussauze, E.I. Kamitsos, C.P.E. Varsamis, D. Ehrt, Thermal poling induced structural changes in sodium borosilicate glasses, Physics and Chemistry of Glasses - European Journal of Glass Science andTechnology Part B, 50 (2009) 229-235.
[72] C.T. Kirk, Quantitative analysis of the effect of disorder-induced mode coupling on infrared absorption in silica, Phys Rev B Condens Matter, 38 (1988) 1255-1273.
[73] J. Luo, H. Huynh, C.G. Pantano, S.H. Kim, Hydrothermal reactions of soda lime silica glass – Revealing subsurface damage and alteration of mechanical properties and chemical structure of glass surfaces, Journal of Non-Crystalline Solids, 452 (2016) 93-101.
[74] A.N. Lazarev, Quantum Chemistry of Molecular Systems Relating to The Crystal Chemistry and Lattice Dynamics of Silicates, in: Molecular Approach to Solids, 1998, pp. 1-81.
[75] M. Klevenz, S. Wetzel, M. Trieloff, H.-P. Gail, A. Pucci, Vibrational spectroscopy of SiO on Si(111), physica status solidi (b), 247 (2010) 2179-2184.

[76] H. Kaya, D. Ngo, S. Gin, S.H. Kim, Spectral changes in Si–O–Si stretching band of porous glass network upon ingress of water, Journal of Non-Crystalline Solids, 527 (2020) 119722.
[77] K. Januchta, M.M. Smedskjaer, Indentation deformation in oxide glasses: Quantification, structural changes, and relation to cracking, Journal of Non-Crystalline Solids: X, 1 (2019).
[78] A. Bouzid, K.J. Pizzey, A. Zeidler, G. Ori, M. Boero, C. Massobrio, S. Klotz, H.E. Fischer, C.L. Bull, P.S. Salmon, Pressure-induced structural changes in the network-forming isostatic glassGeSe4: An investigation by neutron diffraction and first-principles molecular dynamics, Physical Review B, 93 (2016).
[79] F.L. Galeener, G. Lucovsky, Longitudinal Optical Vibrations in Glasses: GeO2and SiO2, Physical Review Letters, 37 (1976) 1474-1478.
[80] C. Levelut, R. Le Parc, A. Faivre, B. Champagnon, Influence of thermal history on the structure and properties of silicate glasses, Journal of Non-Crystalline Solids, 352 (2006) 4495-4499.
[81] J. Schaefer, E.H.G. Backus, M. Bonn, Evidence for auto-catalytic mineral dissolution from surface-specific vibrational spectroscopy, Nature Communications, 9 (2018) 3316.
[82] H. Fujiwara, Spectroscopic Ellipsometry, John Wiley & Sons, Ltd., 2007.